Organic & Biomolecular Chemistry

ARTICLE

Push-pull pyropheophorbides for nonlinear optical imaging

Anjul Khadria,[a] Yovan de Coene,[b] Przemyslaw Gawel,[a] Cécile Roche,[a] Koen Clays*[b] and Harry L. Anderson*[a]

Received 00th January 20xx,
Accepted 00th January 20xx

DOI: 10.1039/x0xx00000x

www.rsc.org/

Pyropheophorbide-a methyl ester (PPa-OMe) has been modified by attaching electron-donor and -acceptor groups to alter its linear and nonlinear optical properties. Regioselective bromination of the terminal vinyl position and Suzuki coupling were used to attach a 4-(*N,N*-diethylaminophenyl) electron-donor group. The electron-acceptor dicyanomethylene was attached at the cyclic ketone position through a Knoevenagel condensation. Four different derivatives of PPa-OMe, containing either electron-donor or electron-acceptor groups, or both, were converted to hydrophilic bis-TEG amides to generate a series of amphiphilic dyes. The absorption and emission properties of all the dyes were compared to a previously reported push-pull type porphyrin-based dye and a commercial push-pull styryl dye, FM4-64. Electrochemical measurements reveal that the electron donor group causes a greater decrease in HOMO-LUMO gap than the electron-acceptor. TD-DFT calculations on optimized geometries (DFT) of all four dyes show that the HOMO is mostly localized on the donor, 4-(*N,N*-diethylaminophenyl), while the LUMO is distributed around the chlorin ring and the electron-acceptor. Hyper-Rayleigh scattering experiments show that the first-order hyperpolarizabilities of the dyes increase on attaching either electron-donor or -acceptor groups, having the highest value when both the donor and acceptor groups are attached. Two-photon excited fluorescence (TPEF) and second harmonic generation (SHG) images of the bis-TEG amide attached dyes in lipid monolayer-coated droplets of water-in-oil reveal that the TPEF and SHG involve transition dipole moments in different orientations.

Introduction

Cellular imaging techniques based on nonlinear optical processes such as two-photon excited fluorescence (TPEF) and second harmonic generation (SHG) are gaining prominence because they can probe deeper into the biological tissues, exhibit reduced out of focus fluorophore bleaching and generate less out of focus emitted and scattered light, compared to other optical microscopy techniques.[1-4] Both TPEF and SHG involve simultaneous interaction of two photons with the chromophore; hence, they require a high density of photons delivered by pulsed (typically sub-picosecond) focused laser beams. While TPEF is detected in all directions around the sample, SHG is mostly detected in the forward direction of the incident light. TPEF signals from individual dyes placed in anti-parallel orientation add up, while the overall SHG signal from anti-parallel dyes cancels. The intensity of an SHG signal is dependent on the second-order polar tensor, χ^2 induced when a non-centrosymmetric molecule is placed in a non-centrosymmetric medium.[5-10] SHG is an ideal technique to image interfaces while avoiding background signals from isotropic regions. TPEF takes place *via* two-photon absorption (TPA) and requires population of real excited states, while SHG is a scattering effect that generates light of twice the incident frequency, only involving virtual states. Both TPA and SHG are enhanced when the electric field of the light is polarized in the direction of the transition dipole moment (TDM) of the molecule.[5,11] TPA and SHG have both been used to probe the electric potentials across cellular membranes.[12-17]

Porphyrins and related porphyrinoid chromophores such as chlorins and bacteriochlorins find applications in various fields such as photodynamic therapy (PDT), fluorescence microscopy, chemical sensing, and photovoltaics because they have excellent linear and nonlinear optical properties due to their large π-system, which can be engineered by various structural modifications.[4,18-23] TPA in porphyrin-related compounds has already been applied in PDT.[24,25] Previously, we demonstrated that the TPA efficiency of porphyrin dimers could be significantly increased by attaching electron-donor and -acceptor groups.[26] We found that apart from increased TPA cross-section, donor-acceptor–based porphyrins give a high SHG response.[2] One of our donor-acceptor free-base porphyrins, JR1, is highly voltage-sensitive in comparison to commercial dyes such as FM4-64, Di-4-ANEPPS and RH237 (Fig. 1), which makes it a good candidate to probe electrical potential differences across cellular membranes.[2,14] We studied the effect of individual electron-donating and -accepting groups attached to porphyrin systems on SHG efficiency, and found that the free-base porphyrin core is substantially electron-deficient, making the electron-withdrawing group redundant.[8] It has been previously suggested that porphyrins substituted with phenyl rings at opposite *meso*-positions have ambivalent nature, i.e. they can behave both as a donor and an acceptor to create a push-pull effect when connected with either an acceptor or a donor group at *meso* or β-positions.[27,28] The

[a]*Department of Chemistry, Oxford University, Chemistry Research Laboratory, Mansfield Road, Oxford OX1 3TA, UK. E-mail: harry.anderson@chem.ox.ac.uk*
[b]*Department of Chemistry, University of Leuven, Celestijnenlaan 200 D, 3001 Leuven, Belgium. Email: Koen.Clays@fys.kuleuven.be*

†Electronic Supplementary Information (ESI) available: Details of synthesis, spectroscopy, electrochemistry, hyper-Rayleigh scattering, microscopy, and DFT calculations. See DOI: 10.1039/x0xx00000x

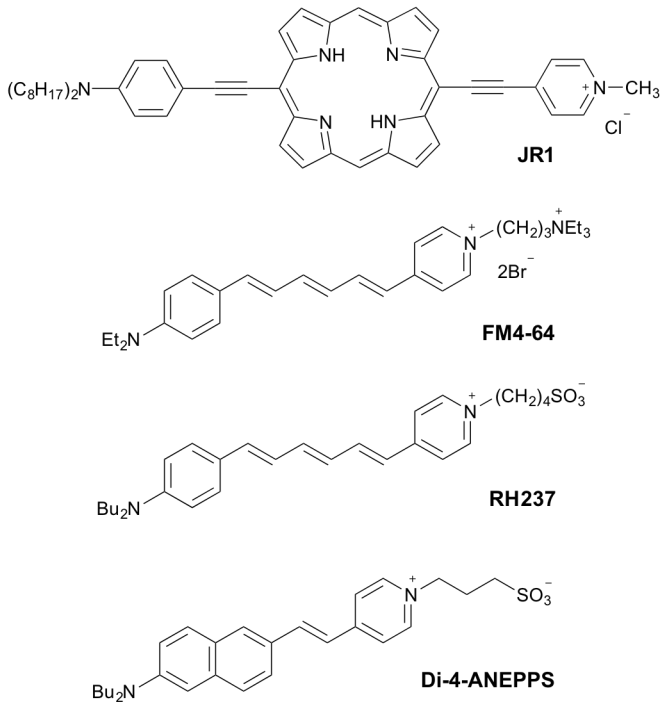

Fig. 1 Molecular structures of voltage-sensitive dyes.[14]

orientations of SHG-based probes within biological membranes play crucial roles for an effective SHG response. Various studies demonstrate different methods to determine the orientation of molecular probes, such as TPEF-based microscopy, solid-state NMR, fluorescence anisotropy, and SHG-based microscopy,[29-33] while we utilized the optical anisotropy of dyes in lipid-based water-in-oil monolayers and bilayers.[11] In this study, we modified the structure of a chlorin molecule, pyropheophorbide-a methyl ester to enhance its linear and nonlinear optical properties.

Pyropheophorbide-a methyl ester (PPa-OMe, **1a**, Fig. 2) is a photosynthetic chlorin obtained by decarboxylation of methyl pheophorbide-a, which is commonly obtained from *Spirulina maxima* algae.[34] Being a non-centrosymmetric π-system, **1a** is expected to give a SHG response when located in a non-centrosymmetric environment. Since it consists of a conjugated macrocycle with several positions available for chemical modifications and creates singlet oxygen with high quantum yield,

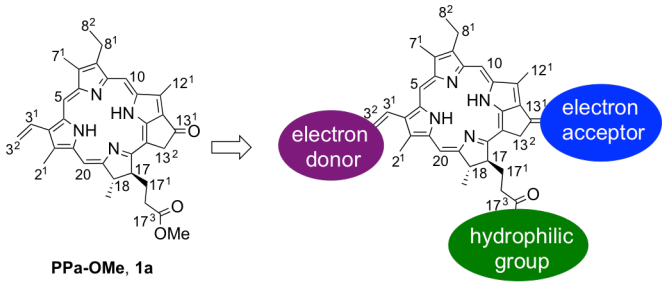

Fig. 2 Modification of pyropheophorbide-a methyl ester (PPa-OMe) for enhanced nonlinear optical properties. Electron-donor, -acceptor and hydrophilic groups are attached at various positions of PPa-OMe.

1a and its derivatives have been extensively studied for *in vitro* and *in vivo* imaging, as well as photodynamic therapy.[35-38] The effects of chemical modification of the π-system of **1a** on its optical properties have been explored in several studies.[39-46] The electronic absorption spectrum of **1a** is characteristic of chlorins, and is dominated by two absorption bands, one in the high-energy region at the border of the UV (Soret band) and one in the far-red visible region (Q band). Absorption in the far-red region is useful for one-photon techniques because photo-damage is reduced at these energies compared to shorter wavelengths. Although the linear optical properties of **1a** and its various derivatives have been widely studied, there are few reports on its nonlinear optical properties.[47,48] The TPA cross-section, σ of **1a** at 800 nm in methanol is only 3.5 GM, which is low compared to many other dyes.[4,24,48,49] It has recently been shown that aggregates of pyropheophorbide-a (**1b**, the acid form of **1a**) give an SHG response.[47] Cui *et al.* formed aggregates of **1b**, organized non-centrosymmetrically in liposomes and studied its optoelectronic properties. They investigated the uptake of **1b**-containing liposomes by live cells and imaged the interior of the cells through SHG and third harmonic generation microscopy.[47]

In order to explore the potential of **1a** as a structural framework for the linear and nonlinear optical imaging of membrane potentials of excitable cells[14,15,50,51] and for imaging biological structures through TPEF and SHG-based microscopy,[2-4,47] we describe the design, synthesis, and properties of a new group of chromophores based on **1a** (Scheme 1). The parent structure of **1a** was modified by attaching electron-donating and -accepting groups to form compounds **2a**, **3a** and **4a**. We aimed to increase the non-centrosymmetry and alter the electronic structure of the parent molecule, to tune its linear and nonlinear optical properties. In order to increase the amphiphilicity of the compound, we also attach a hydrophilic group. We investigate the first-order hyperpolarizability β of the chromophores to study the effect of individual donor and acceptor groups on their SHG efficacies. TD-DFT calculations show that the HOMO is localized on the electron-donor group while the LUMO is localized around the chlorin ring and the acceptor group. While studying the orientation of the compounds in lipid-based water-in-oil monolayer droplets, we found that TPA and SHG in these set of molecules occur through different TDMs.

Results and Discussion

Synthesis

We modified the structure of **1a** (Scheme 1) by attaching electron-donor (4-(*N*,*N*-diethylaminophenyl)) and -acceptor (dicyanomethylene) groups to increase the polarization of its π-system, with the objective of increasing its SHG intensity. We attached a hydrophilic group, bis-triethyleneglycol (TEG) amide, at the carboxylic positions of derivatives of **1a** to make it more amphiphilic and to favor incorporation into lipid membranes.

In order to attach the donor group, we developed a new strategy to selectively brominate at the 3^2-vinyl position of **1a** and then perform Suzuki coupling. Functionalization at the 3^2-position of **1a** is often carried out by oxidation of the vinyl group to an

aldehyde using OsO_4.[43,52] Lonin *et al*. achieved bromination at the 3^2 vinyl position of **1a** by reacting it with Br_2 at –90 °C. The resulting dibromoolefin was heated to eliminate HBr.[53] In our attempts, this procedure was low yielding and gave inconsistent results. Vincente *et al.* used two molar equivalents of *N*-bromosuccinimide (NBS) in the presence of azobisisobutyronitrile (AIBN) on octaethylporphyrin to form *trans*-(2-bromovinyl)-heptaethylporphyrin.[54] Based on this method, we used NBS in the absence of radical initiator to brominate the 3^2-vinyl position of **1a** (Scheme 1), and monitored the reaction by reverse-phase HPLC (RP-HPLC, Fig. S1-A, ESI). Bromination occurs selectively at the 3^2-vinyl position giving **5** in 78% yield. The reaction is stereoselective giving the *E*-product, as evident from the HPLC trace (Figure S1) and ^{1}H NMR spectrum (J = 14.0 Hz; Figure S2). Suzuki coupling was successfully applied (step (ii) in Scheme 1) to attach 4-*(N,N*-diethylaminophenyl) to **5** to give compound **2a.**

Compounds **3a**, **3b** and **4a** were synthesized by attaching malononitrile at the 13^1-carbonyl positions of chlorins **1a**, **1b** and **2a**, respectively, by Knoevenagel condensation.[39,41] This method affords derivatives functionalized with electron-acceptor groups in good yields.

The polar TEG group was attached by first hydrolyzing the methyl esters **2a, 3a** and **4a** to carboxylic acids **2b**, **3b** and **4b** (step (iv), Scheme 1), respectively. Compound **3b** can be formed with higher yield by first performing the Knoevenagel reaction on **1a** to form **3a** and then hydrolyzing the ester rather than directly attaching malononitrile on the carboxylic acid derivative **1b**. The higher isolated yield may be the result of easier purification of the methyl ester derivatives compared to the corresponding carboxylic acids. Compounds **1b**, **2b**, **3b** and **4b** were reacted with bis-TEG amine in the presence of the coupling reagent COMU[55] to form the amphiphilic compounds **1c**, **2c**, **3c** and **4c** (step (v), Scheme 1), respectively.

Linear Optical and Electrochemical Properties

The electronic absorption and emission spectra of all the compounds were measured in dichloromethane solution at 25 °C. The absorption spectra are characteristic of chlorins with Soret bands in the blue region and intense Q bands in the far-red region. The absorption and emission spectra of **1a**, **2a**, **3a** and **4a** (Fig. 3) show a clear effect of functionalization with electron-donating and -accepting groups. The presence of the strongly electron-withdrawing dicyanomethylene group in **3a** causes a greater bathochromic-shift than the electron-donating 4-(*N,N*-diethylaminophenyl) in **2a**. On attaching either electron-donating or accepting groups, the intensity of the Soret band decreases slightly, and absorption in this region becomes structured into a complex pattern of bands. The presence of various transitions within the Soret region is supported by TD-DFT calculations (discussed below). The multiple transition bands in the Soret region of **3a** are of similar intensities unlike the bands of **1a**, **2a** and **4a**. We observe a nearly two-fold increase in intensity of the Q band on attachment of the only acceptor group in **3a**. This effect is not observed on attachment of the donor group (compound **2a**), or of both the donor and acceptor groups (compound **4a**). Similarly, in the emission spectra, a greater bathochromic shift was observed for compound **3a** (with electron-acceptor) than for compound **2a** (with electron-donor), compared to the parent compound **1a**. The emission maximum is further shifted towards a longer wavelength

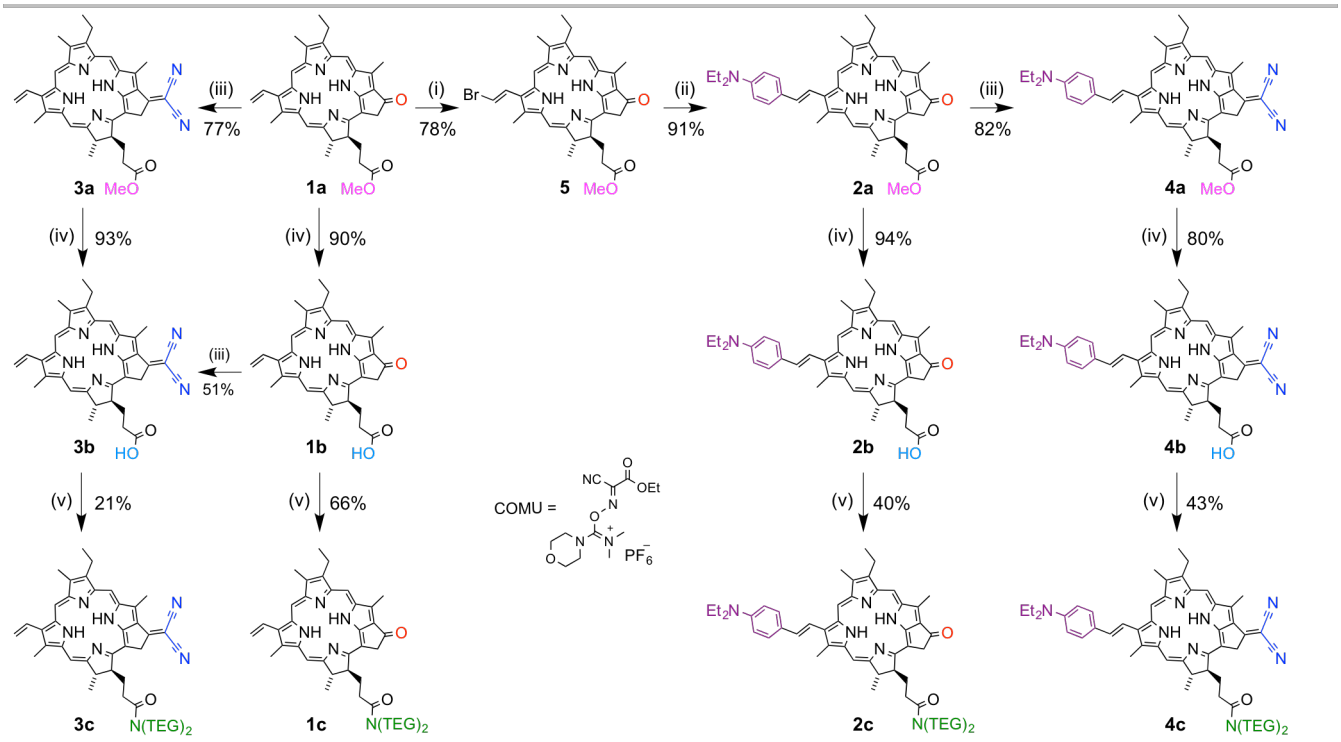

Scheme 1 Synthesis of derivatives of pyropheophorbide-a methyl ester **1a**. Reagents and conditions: (i) *N*-bromosuccinimide (NBS), 1,2-dichloroethane, reflux; (ii) 4-*N,N*-diethylaminophenyl boronic acid, $Pd(PPh_3)_4$, Bu_4NBr, toluene, NaOH (0.2 M aq.), 80 °C; (iii) $CH_2(CN)_2$, Et_3N, reflux; (iv) HCl (aq.), 20 °C; (v) $HN(TEG)_2$, COMU, DMF, iPr_2NEt, 0 °C (TEG: triethyleneglycol).

Table 1 Linear optical properties of **1a–4a** and other dyes

Dye	λ_{max}^{abs} (log ε) / nm	λ_{max}^{em}/nm	ϕ_F	$\Delta\tilde{\nu}$ /eV
1a[a]	413 (5.0), 667 (4.7)	678	0.22[39]	0.030
2a[a]	420 (4.9), 678 (4.7)	689	0.18	0.029
3a[a]	453 (4.9), 704 (5.0)	713	0.24	0.022
4a[a]	458 (4.8), 716 (4.8)	726	0.003	0.023
JR1[2,b]	448 (5.0), 723 (4.9)	803	0.13	1.708
FM4-64[6,b]	564 (4.7)	761	0.35	5.690

[a] in CH_2Cl_2, [b] in $CHCl_3$, $\Delta\tilde{\nu}$ is the Stokes shift, **1a** was used as reference for calculating the fluorescence quantum yields ϕ_F of all other compounds.[39] ε is the molar absorption coefficient in M^{-1} cm^{-1}

when both the electron-donating and -accepting groups are attached in compound **4a**.

The attachment of electron-donor and -acceptor groups did not substantially affect the Stokes shift, which is around 0.025 eV for all compounds. In the PPa-OMe family of dyes (**1a**, **2a**, **3a** and **4a**), the fluorescence quantum yield decreases slightly while substituting with the electron-donating group; however, it increases while attaching the electron-accepting group (Table 1). In the push–pull derivative **4a** the quantum yield decreases by more than 99% (Table 1), which is beneficial for SHG imaging as there is less collateral TPEF. Tamiaki and co-workers have studied the properties of derivatives of **1a** constructed by various functionalizations at its 3^1 and 3^2 positions and attaching malononitrile at its 13^2 position.[39,43] None of those compounds exhibited quantum yields as low as **4a**. It appears that the 4-(*N,N*-diethylaminophenyl) moiety plays a critical role in fluorescence quenching, probably via intramolecular charge transfer.[56-58] We also measured the absorption and emission spectra of **1b**, **2b**, **3b** and **4b** to investigate the effect of the hydrolysis of ester to carboxylic group on the optical properties. This change does not alter the optical properties significantly (Fig. S36).

Table 2 Oxidation and reduction potentials of **1a–4a**[a]

Dye	E^1_{ox} (V)	E^1_{red} (V)	$E_{ox}{}^1$–$E_{red}{}^1$ (V)
1a	0.43	–1.62	2.05
2a	0.17	–1.63	1.80
3a	0.52	–1.38	1.90
4a	0.20	–1.40	1.60

[a] All potentials were measured in THF with 0.1 M NBu_4PF_6, relative to internal ferrocene, Fc/Fc^+ at 0 V.

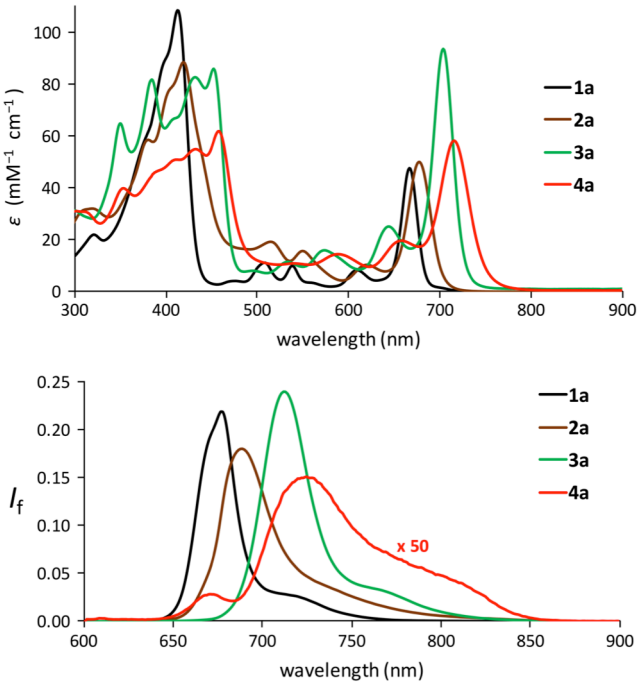

Fig. 3 Absorption and emission spectra of dyes, **1a–4a**. Attaching the electron donor and acceptor groups causes a red shift in the absorption and emission bands, indicating a decrease in the HOMO-LUMO band gap. Measurements were performed in CH_2Cl_2 at 25 °C. For fluorescence measurements, the compounds were excited at their respective Soret bands (414 nm for **1a**, 420 nm for **2a**, 453 nm for **3a**, and 459 nm for **4a**). The fluorescence intensity is normalized such that the areas of the peaks are proportional to their fluorescence quantum yields. The fluorescence intensity for **4a** is multiplied by a factor of 50 for visible comparison

We performed electrochemical measurements (square wave voltammetry) on the chromophores to determine the energies of their frontier orbitals (Table 2, Fig. S37–S40). As expected, the electrochemical HOMO–LUMO gap ($E_{ox}{}^1$ – $E_{red}{}^1$) decreases on attaching electron-donor and -acceptor groups. However, in contrast to the UV-Vis spectra, attachment of the donor group in **2a** decreases the HOMO-LUMO gap more than the acceptor group in **3a**. On attaching the donor group, both the first oxidation and first reduction potentials decrease, while on attaching the acceptor group, they both increase. Tamiaki and co-workers found that on attaching only electron-withdrawing groups (carbonyl and dicyanomethene) at the 13^1 and 3^2 positions of **1a**, the potentials of oxidation and reduction increase, in agreement with our results.[39]

Electronic Structure Calculations

The ground-state geometries of **1a**, **2a**, **3a** and **4a** were optimized by DFT at the B3LYP/6-31G(d) level of theory with solvation in CH_2Cl_2 using the polarizable continuum model (PCM) implemented in the Gaussian09 package (for details see the ESI).[59] On these geometries, vertical optical transitions were calculated by TD-DFT at the B3LYP/LANL2DZ level of theory.[60-62] In the case of **2a** and **4a**, the lowest energy transition (Q band) is found with high precision (difference of 0.06 eV and 0.07 eV, respectively, compared with experiment; Fig. 4). On the contrary, the Q band transition energy of **1a** and **3a** is underestimated by 0.31 eV and 0.30 eV,

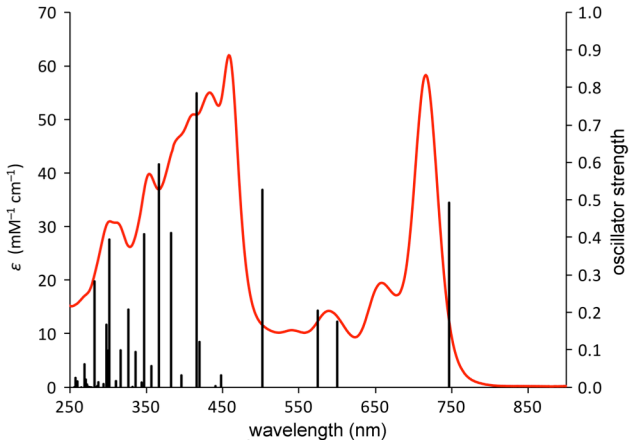

Fig. 4 Overlay of the measured spectrum of **4a** (CH_2Cl_2) and calculated electronic transitions (TD-DFT B3LYP/LANL2DZ, PCM solvation in CH_2Cl_2).

respectively. The splitting of the Soret band into multiple transitions in the higher energy region was predicted with variable precision and the general shape of the spectra could be reproduced (Fig. 4 and Section S7).

The calculated frontier molecular orbitals show a significant difference in the localization of the HOMO and LUMO in **2a** and **4a** (Fig. 5). This suggests that the HOMO-to-LUMO transitions in these derivatives have intramolecular charge-transfer (ICT) character. In the case of **1a** and **3a**, which do not contain the 4-(*N,N*-diethylaminophenyl) group, both the HOMO and LUMO are located on the central chlorin ring. The fact that the LUMO is localized on the chlorin in **2a**, while the HOMO is localized on the 4-(*N,N*-diethylaminophenyl) group, implies that the chlorin ring can act as an electron-acceptor. The calculated ground-state dipole moments show a strong increase in the order: **1a** (7.6 D), **2a** (12.5 D), **3a** (14.6 D) to **4a** (20.7 D).

Hyper-Rayleigh Scattering

The second-order polarizabilities (β_{HRS}) and the component of β along the molecular-axis (β_{zzz}) were measured for the series of PPa-OMe derivatives **1a–4a** in chloroform at 800 nm and 840 nm by hyper-Rayleigh scattering (Table 3).[63,64] The contribution to the β values of both the donor and acceptor at 800 nm are similar. This contrasts with our previously reported porphyrin-based dyes, where an acceptor does not contribute to the β value.[8] The observed difference between the series of dyes may be due to the nature of the conjugated core (porphyrin *vs.* chlorin). A free-base porphyrin, when substituted with a strong donor group can itself act as an acceptor, making the need of an additional acceptor redundant. However, chlorins have higher electron density than porphyrins, which makes them weaker electron acceptors. The β values increase on attaching either the donor in **2a** or the acceptor in **3a**, which means that the chlorin moiety can act as both the acceptor (for compound **2a**) and the donor (for compound **3a**). The β_{zzz} value of **4a** at 800 nm is about half that of the previously studied porphyrin-based SHG voltage sensitive dye, JR1.[2,14] However, it is more than the value that we measured in the same conditions for the commercial SHG dye, FM4-64 (Table 3). The donor and acceptor groups in JR1 are attached at *meso*-positions, whereas, in **4c** they are attached to the chlorin ring at the *beta*-positions. This change of conjugation path undoubtedly contributes towards the difference in HRS behavior.

Table 3 Nonlinear optical properties [a]

Dye	β_{zzz} (λ)/10^{-30} esu (nm)	β_{HRS} (λ)/10^{-30} esu (nm)
1a	350 ± 50 (800), 1760 ± 340 (840)	140 ± 30 (800), 730 ± 140 (840)
2a	790 ± 150 (800), 2700 ± 500 (840)	330 ± 60 (800), 1100 ± 200 (840)
3a	800 ± 150 (800), 3200 ± 560 (840)	330 ± 60 (800), 1300 ± 200 (840)
4a	1330 ± 240 (800), 4700 ± 800 (840)	550 ± 100 (800), 2000 ± 340 (840)
JR1[2]	2300 ± 150 (800), 5800 ± 200 (840)	970 ± 50 (800), 2440 ± 70 (840)
FM4-64	1150 ± 220 (800)	470 ± 90 (800)

[a] All measurements in chloroform

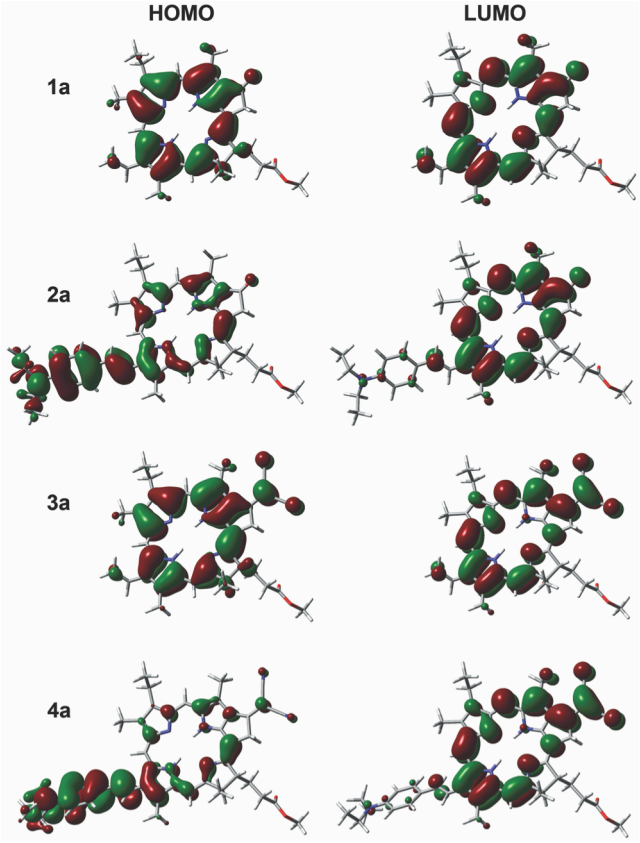

Fig. 5 Frontier molecular orbitals of **1a**, **2a**, **3a** and **4a** at the B3LYP/6-31G(d) level of theory. 0.02 isovalue.

Multi-Photon Microscopy

We imaged the amphiphilic dyes, **1c–4c**, in droplets of water in oil encapsulated by a lipid monolayer using a multi-photon microscope, to test their suitability for SHG and TPEF imaging, and

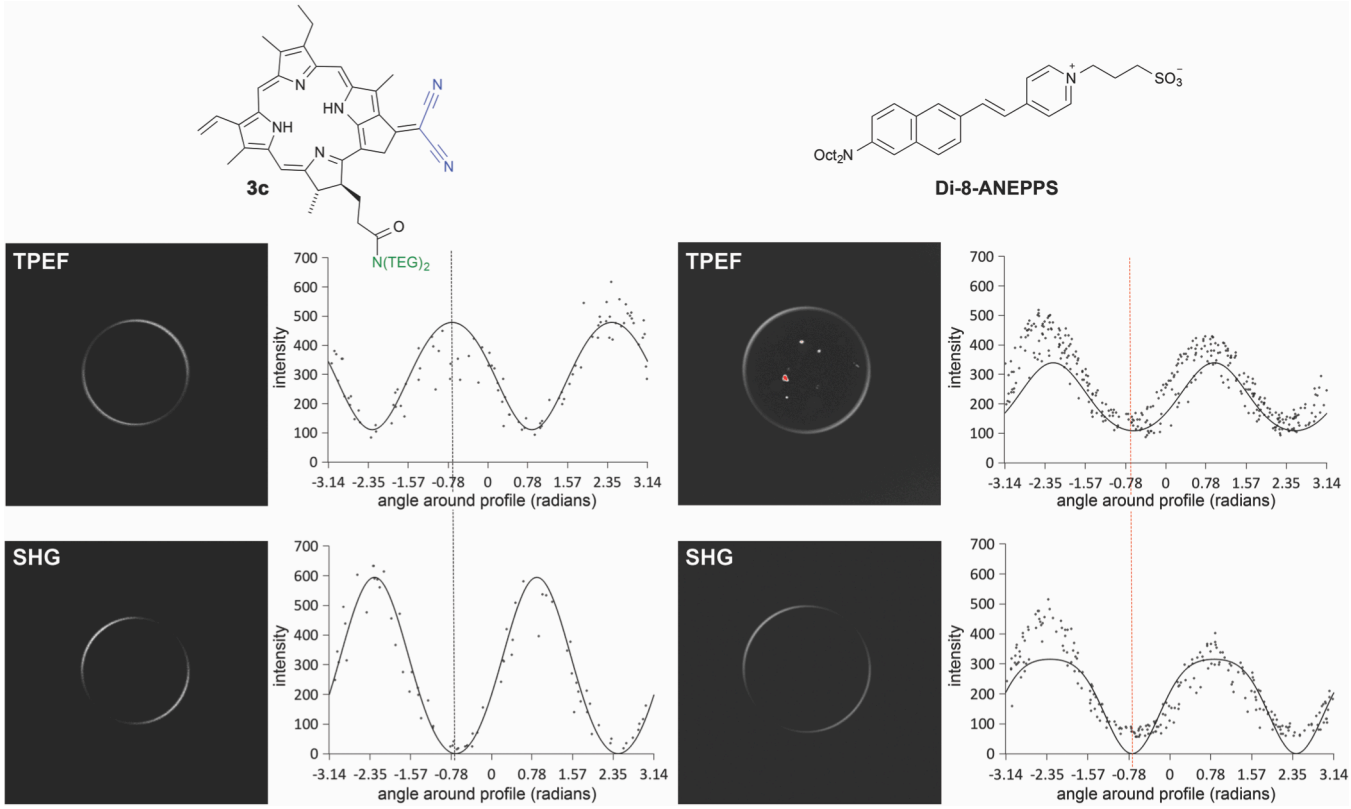

Fig. 6 Two-photon excited fluorescence (TPEF) second harmonic generation (SHG) images of **3c** and Di-8-ANEPPS. The cusp shape of TPEF and SHG are in different directions for **3c**, while they are in the same direction for Di-8-ANEPPS. The angular based intensity plots describe the change of intensity as a function of the phase angle (angle around the droplet). The black dotted line shows the angle at which the TPEF intensity for compound **3c** is at maximum, but SHG is at minimum. The intensities maxima and minima of TPEF and SHG for Di-8-ANEPPS are the same at the same angle (red dotted line). Droplet diameter: 70 μm (**3c**), 150 μm (Di-8-ANEPPS). λ_{ext} = 840 nm (**3c**), 850 nm (Di-8-ANEPPS).

to study their average orientation (tilt angle) and probability distribution of the orientations. Droplets of phosphate buffer (aqueous phase) were mixed with lipids (DPhPC) and dye, and suspended in dodecane (oil phase) already dissolved with DPhPC lipids. The lipid-based water-in-oil monolayer droplets are a simple model for cell membranes, which we previously used to calculate the average tilt angle and probability distribution of the tilt of SHG-based dyes.[11] The amphiphilic dyes locate at the water-oil interface of the spherical droplets. All four compounds give clear SHG images, and the SHG signal is brightest for the push-pull dye **4c**. Upon imaging under the multi-photon microscope, two distinct dark regions are observed around the edge of the droplets where the TDM of the dye is perpendicular to the direction of the polarization of the excitation light, and two bright regions where the TDM is parallel to the polarization of the excitation light (Fig. 6). To calculate the average tilt angle and their distribution in monolayers, we used the previously reported model and software.[11] The model is based on anisotropy data obtained from at least two of the following imaging techniques: one-photon fluorescence, TPEF and SHG (TPEF and SHG used here). Since the model determines the probability distribution of the average tilt angle, it gives information about the preferred tilt (the angle which has the highest probability). The model is based on photoselection rules, which have the primary requirement that the molecule must have a single active TDM at the excitation wavelength. Aiming to obtain average tilt angles and probability distribution of **1c**, **2c**, **3c** and **4c**, through their TPEF and SHG images, we attempted to fit the images using our MATLAB-based image processing software.[11] In **3c**, we found that the intensity maxima (bright regions) and minima (dark regions) of SHG are shifted from their counterparts in TPEF. These results suggest that at the wavelength of excitation (840 nm), **3c** has different TDMs active for TPA and SHG. We compared the change of phase angles (angle around the droplet at which the intensity is at maximum or minimum) for TPA and SHG of **3c** with that of Di-8-ANEPPS, an SHG-based dye, which we used previously to demonstrate our model for measuring the probability distribution of tilt angles (Fig. 6). Di-8-ANEPPS is a linear molecule with a single dominant TDM, which makes it a good candidate for comparison. No shift in the phase angles was observed in the droplets imaged with Di-8-ANEPPS. The phase angles of **1c**, **2c** and **4c** in SHG and TPEF were also slightly shifted from each other when processed in the MATLAB-based software. Hence, we presume that these chromophores also have different TDMs active for TPEF and SHG. TD-DFT calculations predicted that **1c**, **2c** and **4c** have several TDMs (Section S7.2, ESI). This circumstance makes our model unsuitable to measure the probability distribution of tilt angles because it is based on the assumption that both TPEF and SHG are occurring through the same TDM and requires the use of both

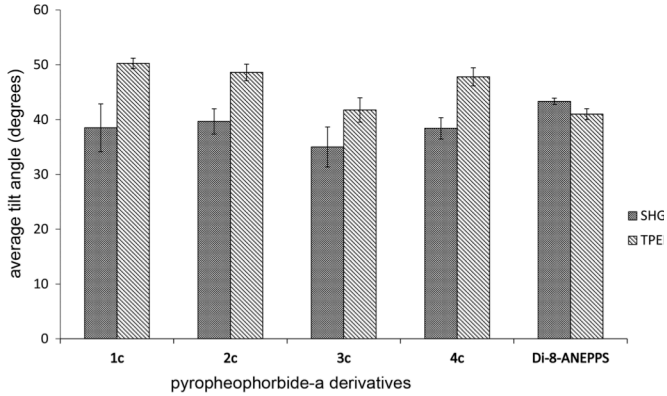

Fig. 7 Comparison of average tilt angles obtained from TPEF and SHG images. The average tilt angle obtained from the TPEF and SHG images for **1c**, **2c**, **3c** and **4c** differ by more than 20%, while the difference for Di-8-ANEPPS is around 5%. This means that there are different TDMs active for TPA and SHG for **1c**, **2c**, **3c** and **4c** but same TDM for Di-8-ANEPPS. The angles decrease on attaching the electron-acceptor group, while they increase on attaching the electron donor group. Error bars represent standard deviation ($n \geq 4$; $n_{\text{Di-8-ANEPPS}} = 3$; n = number of samples).

techniques. Nonetheless, the individual TPEF and SHG images can be used to determine their individual average tilt angles (angle between the active TDM and the normal to the membrane plane), assuming that all the molecules in the droplet orient at the same tilt angle.[11] We processed the TPEF and SHG images of **1c**, **2c**, **3c** and **4c** and fitted the model in order to calculate their respective average tilt angles (Fig. 7). These average tilt angles obtained individually by TPEF and SHG images differ by more than 20% for all the dyes. The value of tilt does not change substantially on attaching the donor group (**1c** to **2c**) but decreases on attaching the acceptor group (**1c** to **3c**) and remains similar on attaching both the donor and acceptor groups (**1c** to **4c**). The average tilt angle from SHG for all the compounds vary between 30° to 40°, while that of TPEF varies between 40° to 50° (Fig. 7). We also processed the TPEF and SHG images of Di-8-ANEPPS as a control experiment, for which the average tilt angles for both TPEF and SHG were found to be the same (the difference of around 5% lies within experimental error). In the PPa-OMe family dyes, SHG is most likely to be resonance enhanced by the TDM lying in the donor-acceptor axis (long axis of the molecule) as evident from the change of β_{zzz} value on attaching individual donor and acceptor groups. This means that the information about the orientation of the whole molecule can be predicted from the average tilt angle values of SHG for **1c**, **2c**, **3c** and **4c** (Fig. 8).

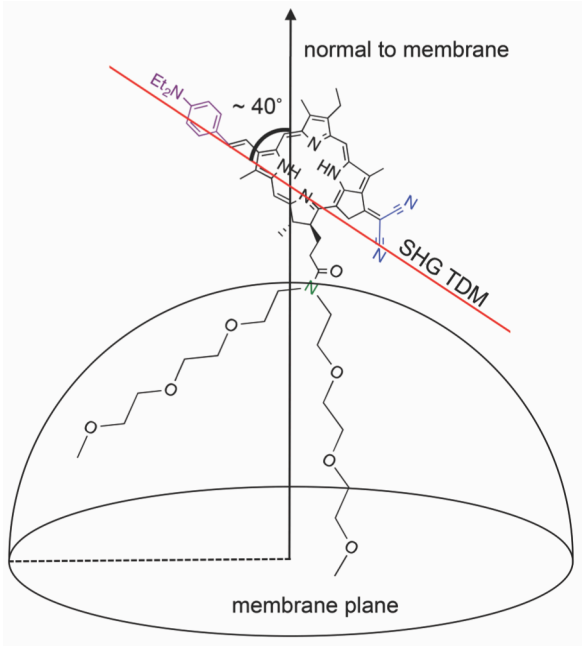

Fig. 8 Physical interpretation of orientation of **4c**, based on the assumption that the average tilt angle of the dye is the angle derived from SHG image.

Since these molecules contain a non-centrosymmetric core macrocycle, they have TDMs pointing at various directions, as shown by TD-DFT calculations (Section S7.2, ESI). To experimentally confirm the existence of various TDM directions at different wavelengths, we measured the polarized fluorescence excitation spectra of **3c** (Fig. S51). This experiment was performed in glycerine-water mixture (9:1), to minimize diffusional reorientation of molecules. The orientation of the polarization filter placed between the sample and the light source was kept constant, while the polarization filter (analyzer) placed between the sample and the detector was rotated by 0° or 90° and the excitation spectrum was measured. The difference in the intensity for these two spectra varies across the UV and visible range, indicating that the direction of TDMs varies at different wavelengths (Fig. S51). This observation is supported by TD-DFT calculations, which show that the TDMs within the Soret band of **3a** are situated at approx. 90°. In contrast to other derivatives, in **3a** the three strong perpendicular transitions dominate the Soret band (Fig. S58 and S59, ESI).

Conclusions

We have synthesized donor-acceptor functionalized amphiphilic derivatives of pyropheophorbide-a methyl ester and studied their linear and nonlinear optical properties in organic solutions and at water-in-oil droplet interfaces. We demonstrated a new approach to functionalize the 3^2-vinyl position of pyropheophorbide-a methyl ester **1a** *via* a regioselective bromination. This approach gives high yields, and could prove useful for the introduction of a wide range of functional groups. The electronic absorption and emission spectra of all the derivatives are characteristic for chlorins. The push-pull substitution pattern results in a strong red-shift in the absorption and fluorescence spectra, with a corresponding reduction in the electrochemical HOMO-LUMO gap and an increase in the hyperpolarizability β, measured by hyper-Rayleigh scattering. The fluorescence quantum yield of the push-pull derivative **4a** is drastically reduced, possibly due to photoinduced charge-separation. Analysis of the TPEF and SHG images of lipid-monolayer coated droplets containing these dyes shows that the TDMs dominating the SHG are sometimes orthogonal to those responsible for two-photon absorption, depending on the wavelength of excitation. The presence of several almost perpendicular TDMs was confirmed by TD-DFT calculations and by polarized fluorescence excitation spectra. Since the SHG of a dye depends on the orientation of its

dominant TDM, control of the orientation of the TDMs is crucial in the design of a SHG dye. Amphiphilic chromophores based on **4c** are promising prototypes for voltage-sensitive dyes for monitoring membrane potential in excitable cells such as neurons.

Acknowledgements

We thank the Engineering and Physical Sciences Research Council (EPSRC) for support, and the John Fell fund and the EP Abraham Cephalosporin Fund, University of Oxford, for partly funding a multi-photon microscope. A.K. acknowledges the Systems Approaches to Biomedical Sciences and Systems Biology Doctoral Training Center, the Clarendon Scholarships Fund, Hilla Ginwala Scholarships, Radhakrishnan Memorial Fund, and St. Catherine's College Overseas Graduate Scholarships at the University of Oxford. We thank Wojciech Kaluza and Shifali Shishodia (both University of Oxford), and Carmen Bartic and Veerle Baekelandt (both University of Leuven) for valuable discussion. Y.C. thanks the Government of Flanders (Belgium) for an IWT Scholarship. P.G. acknowledges the receipt of an Early Postdoc Mobility fellowship from the Swiss National Science Foundation (SNF). *The authors would like to acknowledge the use of the University of Oxford Advanced Research Computing (ARC) facility in carrying out the computational work. http://dx.doi.org/10.5281/zenodo.22558.*

Notes and references

1. M. Scanziani and M. Häusser, *Nature*, 2009, **461**, 930-939.
2. J. E. Reeve, H. A. Collins, K. De Mey, M. M. Kohl, K. J. Thorley, O. Paulsen, K. Clays and H. L. Anderson, *J. Am. Chem. Soc.*, 2009, **131**, 2758-2759.
3. K. Svoboda and R. Yasuda, *Neuron*, 2006, **50**, 823-839.
4. M. Pawlicki, H. A. Collins, R. G. Denning and H. L. Anderson, *Angew. Chem. Int. Ed.*, 2009, **48**, 3244-3266.
5. T. Verbiest, S. Houbrechts, M. Kauranen, K. Clays and A. Persoons, *J. Mater. Chem.*, 1997, **7**, 2175-2189.
6. I. López-Duarte, P. Chairatana, Y. Wu, J. Pérez-Moreno, P. M. Bennett, J. E. Reeve, I. Boczarow, W. Kaluza, N. A. Hosny, S. D. Stranks, R. J. Nicholas, K. Clays, M. K. Kuimova and H. L. Anderson, *Org. Biomol. Chem.*, 2015, **13**, 3792-3802.
7. T. Cañeque, A. M. Cuadro, J. Alvarez-Builla, J. Pérez-Moreno, K. Clays, O. Castaño, J. L. Andrés and J. J. Vaquero, *Dyes and Pigm.*, 2014, **101**, 116-121.
8. I. López-Duarte, J. E. Reeve, J. Pérez-Moreno, I. Boczarow, G. Depotter, J. Fleischhauer, K. Clays and H. L. Anderson, *Chem. Sci.*, 2013, **4**, 2024-2027.
9. C. Barsu, R. Cheaib, S. Chambert, Y. Queneau, O. Maury, D. Cottet, H. Wege, J. Douady, Y. Bretonnière and C. Andraud, *Org. Biomol. Chem.*, 2010, **8**, 142-150.
10. V. Parthasarathy, R. Pandey, M. Stolte, S. Ghosh, F. Castet, F. Würthner, P. K. Das and M. Blanchard-Desce, *Chem. Eur. J.*, 2015, **21**, 14211-14217.
11. J. E. Reeve, A. D. Corbett, I. Boczarow, T. Wilson, H. Bayley and H. L. Anderson, *Biophys. J.*, 2012, **103**, 907-917.
12. P. Theer, W. Denk, M. Sheves, A. Lewis and P. B. Detwiler, *Biophys. J.*, 2011, **100**, 232-242.
13. M. Nuriya, S. Fukushima, A. Momotake, T. Shinotsuka, M. Yasui and T. Arai, *Nat. Commun.*, 2016, **7**, 11557.
14. J. E. Reeve, A. D. Corbett, I. Boczarow, W. Kaluza, W. Barford, H. Bayley, T. Wilson and H. L. Anderson, *Angew. Chem. Int. Ed.*, 2013, **52**, 9044-9048.
15. J. Jiang, K. B. Eisenthal and R. Yuste, *Biophys. J.*, 2007, **93**, L26-L28.
16. J. A. N. Fisher and B. M. Salzberg, in *Membrane Potential Imaging in the Nervous System and Heart*, eds. M. Canepari, D. Zecevic and O. Bernus, *Springer*, 2015, **859**, 427-453.
17. D. A. Dombeck, L. Sacconi, M. Blanchard-Desce and W. W. Webb, *J. Neurophysiol.*, 2005, **94**, 3628-3636.
18. T. K. Ahn, K. S. Kim, D. Y. Kim, S. B. Noh, N. Aratani, C. Ikeda, A. Osuka and D. Kim, *J. Am. Chem. Soc.*, 2006, **128**, 1700-1704.
19. K. Kurotobi, K. S. Kim, S. B. Noh, D. Kim and A. Osuka, *Angew. Chem. Int. Ed.*, 2006, **45**, 3944-3947.
20. K. S. Kim, J. M. Lim, A. Osuka and D. Kim, *J. Photochem. Photobiol. C Photochem. Rev.*, 2008, **9**, 13-28.
21. E. Secret, M. Maynadier, A. Gallud, A. Chaix, E. Bouffard, M. Gary-Bobo, N. Marcotte, O. Mongin, K. El Cheikh, V. Hugues, M. Auffan, C. Frochot, A. Morère, P. Maillard, M. Blanchard-Desce, M. J. Sailor, M. Garcia, J.-O. Durand and F. Cunin, *Adv. Mater.*, 2014, **26**, 7643-7648.
22. C. M. Lemon, E. Karnas, M. G. Bawendi and D. G. Nocera, *Inorg. Chem.*, 2013, **52**, 10394-10406.
23. Y. Mi, P. Liang, Z. Yang, D. Wang, H. Cao, W. He and H. Yang, *Chem. Res. Chin. Univ.*, 2015, **31**, 992-996.
24. M. Khurana, H. A. Collins, A. Karotki, H. L. Anderson, D. T. Cramb and B. C. Wilson, *Photochem. Photobiol.*, 2007, **83**, 1441-1448.
25. M. K. Kuimova, H. A. Collins, M. Balaz, E. Dahlstedt, J. A. Levitt, N. Sergent, K. Suhling, M. Drobizhev, N. S. Makarov, A. Rebane, H. L. Anderson and D. Phillips, *Org. Biomol. Chem.*, 2009, **7**, 889-896.
26. J. D. Wilkinson, G. Wicks, A. Nowak-Król, Ł. G. Łukasiewicz, C. J. Wilson, M. Drobizhev, A. Rebane, D. T. Gryko and H. L. Anderson, *J. Mater. Chem. C*, 2014, **2**, 6802-6809.
27. E. Annoni, M. Pizzotti, R. Ugo, S. Quici, T. Morotti, M. Bruschi and P. Mussini, *Eur. J. Inorg. Chem.,* 2005, 3857-3874.
28. T. Morotti, M. Pizzotti, R. Ugo, S. Quici, M. Bruschi, P. Mussini and S. Righetto, *Eur. J. Inorg. Chem.*, 2006, 1743-1757.
29. P. Ferrand, P. Gasecka, A. Kress, X. Wang, F. Z. Bioud, J. Duboisset and S. Brasselet, *Biophys. J.*, 2014, **106**, 2330-2339.
30. R. A. Badley, H. Schneide and W. G. Martin, *Biochem. Biophys. Res. Commun.*, 1971, **45**, 174-183.
31. B. Corry, D. Jayatilaka, B. Martinac and P. Rigby, *Biophys. J.,* 2006, **91**, 1032-1045.
32. R. S. Ries, H. Choi, R. Blunck, F. Bezanilla and J. R. Heath, *J. Phys. Chem. B*, 2004, **108**, 16040-16049.
33. U. A. Vanderheide, B. Orbons, H. C. Gerritsen and Y. K. Levine, *Eur. Biophys. J. Biophys. Lett.*, 1992, **21**, 263-272.
34. K. M. Smith, D. A. Goff and D. J. Simpson, *J. Am. Chem. Soc.*, 1985, **107**, 4946-4954.

35. J. F. Lovell, C. S. Jin, E. Huynh, H. Jin, C. Kim, J. L. Rubinstein, W. C. W. Chan, W. Cao, L. V. Wang and G. Zheng, *Nat. Mater.*, 2011, **10**, 324-332.
36. V. Tassetti, A. Hajri, M. Sowinska, S. Evrard, F. Heisel, L. Q. Cheng, J. A. Miehe, J. Marescaux and M. Aprahamian, *Photochem. Photobiol.*, 1997, **65**, 997-1006.
37. P. Keller, M. Sowinska, V. Tassetti, F. Heisel, A. Hajri, S. Evrard, J. A. Miehe, J. Marescaux and M. Aprahamian, *Photochem. Photobiol.*, 1996, **63**, 860-867.
38. A. P. Castano, P. Mroz and M. R. Hamblin, *Nat. Rev. Cancer*, 2006, **6**, 535-545.
39. S. Sasaki, M. Yoshizato, M. Kunieda and H. Tamiaki, *Eur. J. Org. Chem.,* 2010, 5287-5291.
40. G.-F. Han, J.-J. Wang and Y. K. Shim, *J. Photosci.*, 2001, **8**, 71-73.
41. J. J. Wang, J. Z. Li, J. Jakus and Y. K. Shim, *J. Porphyrins Phthalocyanines*, 2012, **16**, 122-129.
42. I. Stamati, M. K. Kuimova, M. Lion, G. Yahioglu, D. Phillips and M. P. Deonarain, *Photochem. Photobiol. Sci.*, 2010, **9**, 1033-1041.
43. H. Tamiaki, M. Kuno and M. Ohata, *Photochem. Photobiol.*, 2014, **90**, 1277-1286.
44. H. Tamiaki, K. Fukai, H. Shimazu and S. Shoji, *Photochem. Photobiol.*, 2014, **90**, 121-128.
45. I. Ghosh, N. Saleh and W. M. Nau, *Photochem. Photobiol. Sci.*, 2010, **9**, 649-654.
46. Y. Chen, X. Zheng, M. P. Dobhal, A. Gryshuk, J. Morgan, T. J. Dougherty, A. Oseroff and R. K. Pandey, *J. Med. Chem.*, 2005, **48**, 3692-3695.
47. L. Cui, D. Tokarz, R. Cisek, K. K. Ng, F. Wang, J. Chen, V. Barzda and G. Zheng, *Angew. Chem. Int. Ed.*, 2015, **54**, 13928-13932.
48. T. Luo, B. C. Wilson and Q.-B. Lu, *J. Photochem. Photobiol. B-Biol.*, 2014, **132**, 102-110.
49. H. A. Collins, M. Khurana, E. H. Moriyama, A. Mariampillai, E. Dahlstedt, M. Balaz, M. K. Kuimova, M. Drobizhev, V. X. D. Yang, D. Phillips, A. Rebane, B. C. Wilson and H. L. Anderson, *Nat. Photonics*, 2008, **2**, 420-424.
50. D. A. Dombeck, M. Blanchard-Desce and W. W. Webb, *J. Neurosci.*, 2004, **24**, 999-1003.
51. A. C. Millard, L. Jin, A. Lewis and L. M. Loew, *Opt. Lett.*, 2003, **28**, 1221-1223.
52. H. Tamiaki, S. Miyata, Y. Kureishi and R. Tanikaga, *Tetrahedron*, 1996, **52**, 12421-12432.
53. I. S. Lonin, A. S. Kuzovlev, E. S. Belyaev, G. V. Ponomarev, O. I. Koifman and A. Y. Tsivadze, *J. Porphyrins Phthalocyanines*, 2014, **18**, 123-128.
54. M. G. H. Vicente and K. M. Smith, *Tetrahedron*, 1991, **47**, 6887-6894.
55. A. El-Faham and F. Albericio, *J. Pept. Sci.,* 2010, **16**, 6-9.
56. S. Sasaki, G. P. C. Drummen and G. Konishi, *J. Mater. Chem. C*, 2016, **4**, 2731-2743.
57. J. B. Kelber, N. A. Panjwani, D. Wu, R. Gómez-Bombarelli, B. W. Lovett, J. J. L. Morton and H. L. Anderson, *Chem. Sci.*, 2015, **6**, 6468-6481.
58. A. Kahnt, J. Kärnbratt, L. J. Esdaile, M. Hutin, K. Sawada, H. L. Anderson and B. Albinsson, *J. Am. Chem. Soc.*, 2011, **133**, 9863-9871.
59. Gaussian 09, Revision **D.01**, M. J. Frisch, G. W. Trucks, H. B. Schlegel, G. E. Scuseria, M. A. Robb, J. R. Cheeseman, G. Scalmani, V. Barone, B. Mennucci, G. A. Petersson, H. Nakatsuji, M. Caricato, X. Li, H. P. Hratchian, A. F. Izmaylov, J. Bloino, G. Zheng, J. L. Sonnenberg, M. Hada, M. Ehara, K. Toyota, R. Fukuda, J. Hasegawa, M. Ishida, T. Nakajima, Y. Honda, O. Kitao, H. Nakai, T. Vreven, J. A. Montgomery, Jr., J. E. Peralta, F. Ogliaro, M. Bearpark, J. J. Heyd, E. Brothers, K. N. Kudin, V. N. Staroverov, R. Kobayashi, J. Normand, K. Raghavachari, A. Rendell, J. C. Burant, S. S. Iyengar, J. Tomasi, M. Cossi, N. Rega, J. M. Millam, M. Klene, J. E. Knox, J. B. Cross, V. Bakken, C. Adamo, J. Jaramillo, R. Gomperts, R. E. Stratmann, O. Yazyev, A. J. Austin, R. Cammi, C. Pomelli, J. W. Ochterski, R. L. Martin, K. Morokuma, V. G. Zakrzewski, G. A. Voth, P. Salvador, J. J. Dannenberg, S. Dapprich, A. D. Daniels, Ö. Farkas, J. B. Foresman, J. V. Ortiz, J. Cioslowski, and D. J. Fox, Gaussian, Inc., Wallingford CT, 2009.
60. P. J. Hay and W. R. Wadt, *J. Chem. Phys.*, 1985, **82**, 299-310.
61. P. J. Hay and W. R. Wadt, *J. Chem. Phys.*, 1985, **82**, 270-283.
62. W. R. Wadt and P. J. Hay, *J. Chem. Phys.*, 1985, **82**, 284-298.
63. K. Clays and A. Persoons, *Phys. Rev. Lett.*, 1991, **66**, 2980-2983.
64. K. Clays, E. Hendrickx, M. Triest, T. Verbiest, A. Persoons, C. Dehu and J. L. Brédas, *Science*, 1993, **262**, 1419-1422.